INVESTIGATION OF SURFACE AND BULK PROCESSES IN Mg-BASED ALLOYS DURING HYDROGEN ABSORPTION

Balázs Vehovszky [1,*], Ágnes Cziráki [2]

[1] Budapest University of Technology and Economics, Department of Vehicle Manufacturing and Repairing, H-1111 Budapest, Műegyetem rkp. 3., Hungary.
[2] Eötvös Loránd University, Department of Materials Physics, H-1117 Budapest, Pázmány Péter sétány 1/a, Hungary.
[*] corresponding author: e-mail: vehovszky@kgtt.bme.hu

Resume

Different Mg-based alloys were tailored and prepared to investigate the surface and bulk processes during hydrogen absorption. Volumetric-, resistance-, XRD-, optical-, and mass measurements were carried out. Heat treatment experiments showed that the short-term thermal stability limits (during heating up at 5 K/min) of the amorphous samples were between 125-175 ° C, while long-term stability (during 24h heat treatment) is always lower – between 80 and 150°C. Nanocrystalline alloys were stable up to 300°C. Hydrogen absorption measurements were executed between 25 and 300°C. Pd-containing alloys were found to be the fastest absorbers, and 200°C was the optimal temperature regarding absorption rate. Etching the samples previously in HF solution enhances absorption by inducing surface cracking. This phenomenon was thoroughly examined by optical microscopy. The effect of hydrogen on the crystallization properties of MgNiPd sample was determined via in-situ resistance measurements.

Available online: http://fstroj.uniza.sk/journal-mi/PDF/2012/19-2012.pdf

Article info

Article history:
Received 2 May 2012
Accepted 17 June 2012
Online 30 September 2012

Keywords:
Magnesium hydrogen storage;
Melt-spinning;
Absorption kinetics;
Surface processes;
Crystallization

ISSN 1335-0803 (print version)
ISSN 1338-6174 (online version)

1. Introduction

Hydrogen absorbing alloys are widely investigated in the last decade aiming an efficient and safe hydrogen storage application for mobile energy sources. Mg and its alloys are among the most promising absorbent materials, having maximum 7.6 wt. % storage capacity [1]; however, the conditions of their application (pressure, temperature) are difficult to realize under industrial conditions. Alloying elements as well as special preparation techniques are used for ameliorating the thermodynamics and kinetics of absorption and desorption. The investigations are usually based on empirical results; thorough examinations – which could point out the potential improvements and make research more efficient – are rarely performed. Moreover, the examination methods and conditions are very different, thus experimental results could not be compared objectively.

Our first aim was to prepare and investigate the most promising Mg-based alloys under the same conditions as reported in the literature – allowing us to collate separately the effect of different alloying elements on the absorption properties.

The second aim of our examination was to investigate the characteristic processes of H-absorption under sterile conditions – without any considerable contamination and extraordinary surface effects, in single-phase samples. It is possible with rapidly solidified, amorphous samples, which absorb hydrogen as solid solution. Although specific surface area is much smaller and diffusion distances are longer than at pulverized samples – thus worse kinetics are expected, surface and bulk processes can be examined efficiently with simple methods and common equipments.

2. Experimental

2.1. Sample preparation

Investigated ribbons were tailored according to absorption experimental results in the literature [1]. The general composition was $Mg_{87}Ni_{10}Me_3$, where Me was Co, Cr, Cu, Fe, La, Ni, Pd, V and MM (mischmetal), which is a Ce-rich rare earth metal alloy, a waste material of FeSiMg production. Another technical alloy, AZ91 (~90 mass % Mg, 9 mass % Al, 1 mass % Zn and Mn) was also used to prepare $AZ91_{90}Ni_{10}$ alloy. After the first experiments, a quaternary alloy, $Mg_{77}Ni_{17}Pd_3V_3$ and a pure Mg-sample were prepared, too.

In the **first step** of the preparation process, a Ni-Me pre-alloy was prepared in a horizontal, copper cold crucible via high-frequency induction melting under atmospheric Ar-pressure. **The second step** was melting Mg and Ni-Me pre-alloy together in a vertical, boron nitride-coated, induction-heated graphite crucible. To ensure homogeneity, multiple re-melting was applied under 0.6 atm Ar-pressure. **The third step** was the rapid solidification of the alloys via the single-roller melt spinning technology (see Ref. [5] for details) under 0.6 atm Ar atmosphere. The surface velocity of the copper roller was 30 m/s. The molten alloy was shot out from a quartz tube through a 0.6 mm nozzle with 200 mbar Ar overpressure.

The resulting ribbons have a thickness of 20 – 35 μm and a width of 1.5 – 2 mm depending on alloy composition. There were basically amorphous alloys (Pd, Fe, Cu, La, PdV, MM and Ni-containing ribbons) which contain only a slight nanocrystalline Mg-fraction on the free side of the ribbon (which did not contact with the copper roller, thus cooling rate was lower). The other alloys (V, Co, AZ91-containing and pure Mg) were crystalline, while Cr-containing sample contains nanocrystalline particles in an amorphous matrix.

The characteristic geometry of the samples was measured on the cross-sections of the ribbons – shown in Fig. 2.

2.2. Investigation methods

The composition of the ribbons was checked via **EDAX measurement** (Energy Dispersive X-ray measurement). Results show good accordance with preparation parameters, however, a slight inhomogenety was detected (the free surface of the ribbons is enriched in Mg).

Table 1

Microstructure and thermal stability of the samples

Sample	AS-quenched microstructure	Short term thermal stability	Long term thermal stability
$AZ91_{90}Ni_{10}$	crystalline	min. 220 °C	min. 220 °C
$Mg_{87}Ni_{13}$	amorphous	145 °C	< 100 °C
$Mg_{87}Ni_{10}V_3$	crystalline	min. 300 °C	min. 300 °C
$Mg_{87}Ni_{10}Co_3$	crystalline	min. 290 °C	
$Mg_{85}(LaNi_5)_{15}$	amorphous	130 °C	min. 100 °C
$Mg_{87}Ni_{10}Pd_3$	amorphous	140 °C	min. 100 °C (< 150 °C)
$Mg_{87}Ni_{10}Cr_3$	amorphous – nanocryst.	100 °C	
$Mg_{87}Ni_{10}Fe_3$	amorphous	140 °C	
$Mg_{87}Ni_{10}Cu_3$	amorphous	130 °C	
$Mg_{77}Ni_{17}Pd_3V_3$	amorphous	175 °C	min. 100 °C (< 150 °C)
$Mg_{87}Ni_{10}MM_3$	amorphous	120 °C	< 100

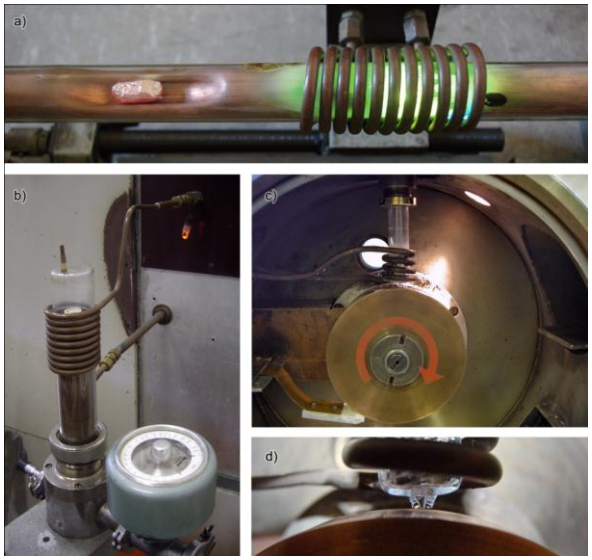

Fig. 1. Sample preparation: Melting pre-alloy in horizontal cold crucible (a), melting in vertical graphite crucible (b), melt-spinning chamber (c) and quartz nozzle (d)
(full colour version available online)

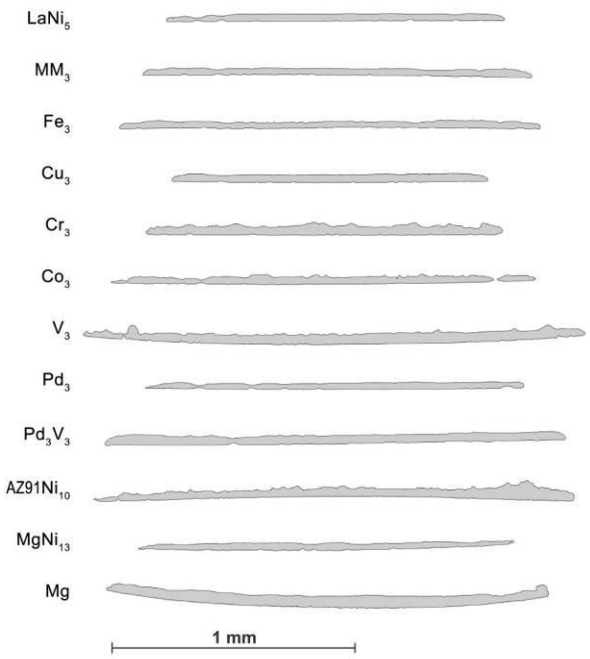

Fig. 2. The cross-section geometry of the ribbons

When an appropriate **surface preparation** is executed before hydrogenation, the long activation process can be avoided at high temperature and high pressure [2]. We found that etching in 10 % HF solution enables the samples for hydrogen uptake. The mechanism of this phenomenon has also been investigated.

Hydrogenation of the samples was carried out in a Sieverts-type apparatus [6] in a pressure range of 1 mbar – 10 bar and temperature range of 25 – 300 °C. Electric resistance of the ribbons were continuously registered during heat treatments and hydrogenations, as it responds very sensitively to structural changes and hydrogen content. For details of the apparatus and principle of measurement see Ref. [3].

The microstructure of the as-quenched and treated samples was investigated via XRD (X-Ray Diffraction) measurements. The volume fraction of different phases was determined by the integral value of the peaks.

Surface processes were examined with a video microscope (Fig. 3). For reaching appropriate images from uneven sample surfaces, focus stacking technology was used – see [7].

3. Results and Discussion

3.1. Physical properties of samples

Density and electrical resistance of the prepared samples were determined. As it is expected, the resistance of amorphous ribbons reaches a value even 20 times higher than those of crystalline ones [8]. The density values were determined by the cross section area, the length and the mass of the ribbons. To reduce measurement error, 3 different cross sections were measured for each sample. (Preliminary tests show that the commonly used hydrostatic density determination method result in a high measuring error – presumably due to the very fine surface topology of the ribbon-sides) Results are shown in Fig. 4. Theoretical densities were calculated assuming Mg_2Ni (density 3.43 g/cm^3 [4]), Mg and Me crystalline phases. It can be seen that most ribbons have lower density compared to the identical theoretical crystalline

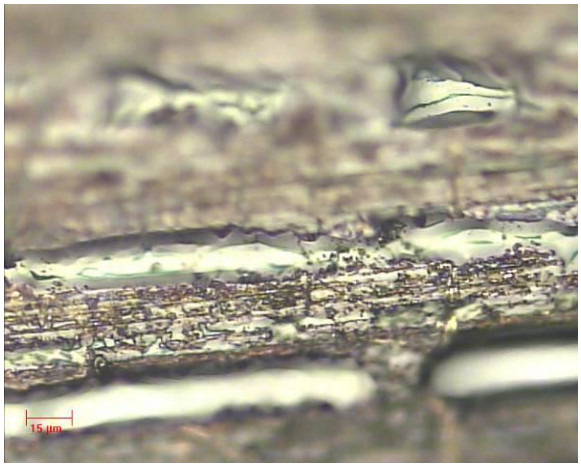

a)

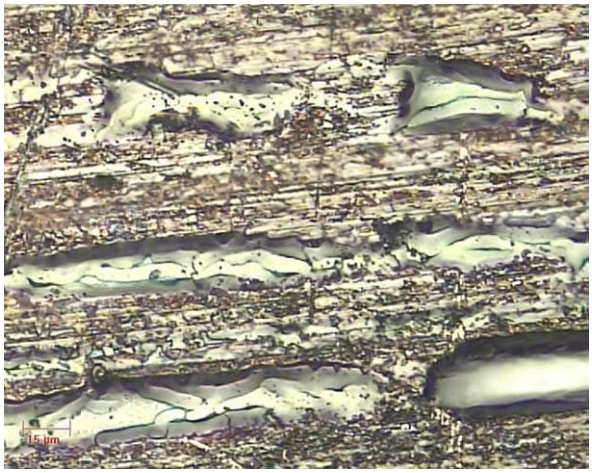

b)

Fig. 3. $Mg_{87}Ni_{13}$ melt spun ribbon surface without (a) and with focus stacking (b)
(full colour version available online)

alloy. This finding is in accordance with *free volume theory* for amorphous alloys [8]. The lower density of crystalline alloys can be explained with the increased proportion of grain boundaries resulted by melt spinning. Pd and La-containing alloys, however, have definitely higher density than corresponding theoretical alloys. The reason of this phenomenon could be that only these two elements – among used alloying metals – form Mg-rich phases (Mg_6Pd and $Mg_{12}La$) which could bond free magnesium in a more dense form. As the ribbons in question are amorphous, it can be concluded that *the nearest-neighbour atomic configurations of an amorphous phase retain the elementary cell of equilibrium phases, which enables shorter atomic distances, thus higher density.*

3.2. Thermal properties of samples

Thermal stability of the samples had to be determined as hydrogenations took place at higher temperatures (up to 300 °C). At most samples it was found that structural changes start at around 150 °C when heating up (short term thermal stability, see Table 1), however, long term thermal stability limits are usually lower – as it can be seen on Fig. 5 in the case

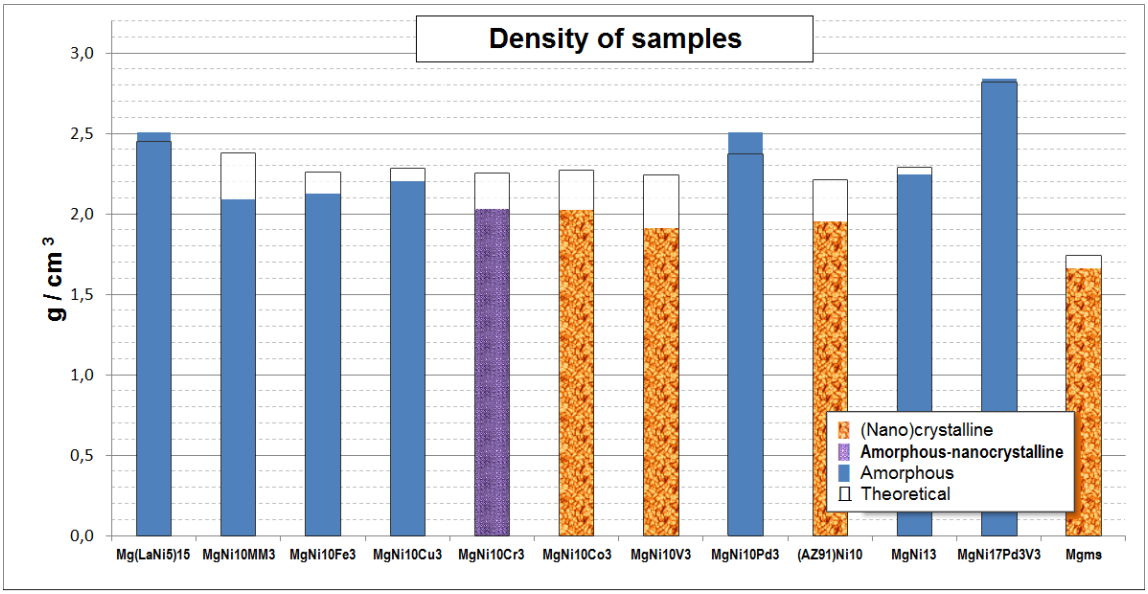

Fig. 4. Measured density of samples (full colour version available online)

of sample $Mg_{87}Ni_{13}$: despite the thermal stability up to 145 °C while heating up, during a long annealing at 100 °C, this sample starts to crystallize, which is obvious from the drop of resistance and the positive thermal coefficient of resistance when cooling down.

Crystallization properties of samples during heat treatment were checked via XRD measurements: as it is shown on Fig. 6, the crystallization of sample $Mg_{87}Ni_{10}Pd_3$ do not start at 100 °C. However, a slight shift of the amorphous peak towards higher angles is determined, which indicates the lowering of average atomic distances in the amorphous structure. This effect is due to the structural relaxation, the lowering of free volumes in the microstructure.

During heat treatment at 200 °C a definite crystallization takes place. The main crystallized phase is Mg_6Pd (77 %) beside 14.4 % amorphous, 6 % Mg_2Ni and few Ni, Mg and Mg_5Pd_2 phases. The high fraction of Mg_6Pd phase confirms the conclusion of density measurement (see the end of section 3.1).

Increasing temperature to 300 °C makes crystallization more pronounced: narrower peaks refer to larger grain size; however, the same phases are formed as during treatment at 200 °C, and an amorphous fraction (around 5 %) still remains. (All samples were heat treated under 5 atm Ar for 24 hours.)

3.3. Surface preparation

Etching samples in 10 % HF solution before hydrogenation was found to speed up hydrogen uptake (see Fig. 7). The mechanism of this surface activation has been suggested in [10] for Zr-based glassy alloys: on one hand, HF removes Zr-oxide, on the other hand, surface get rich in alloying elements, as Ni, Pd, Cr etc. Additional effect is the growing specific surface area.

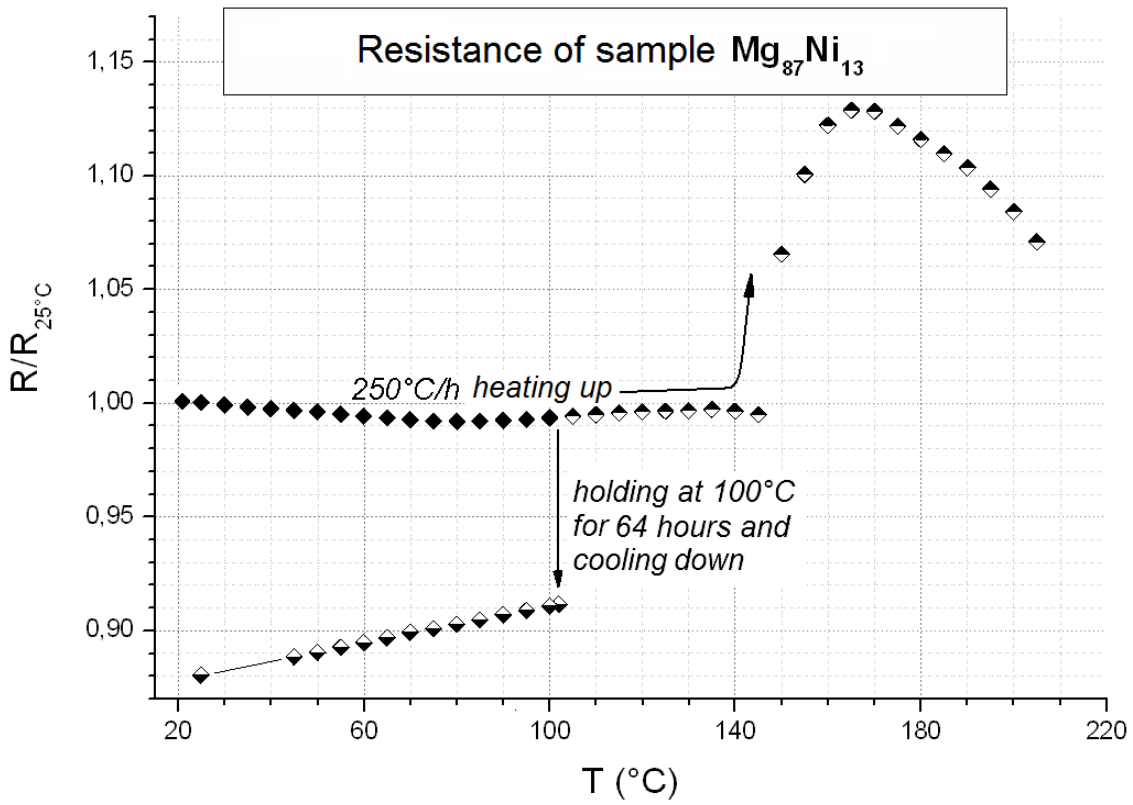

Fig. 5. Change of resistance during heating up and heat treatment at 100 °C – sample $Mg_{87}Ni_{13}$ (amorphous in as-quenched state)

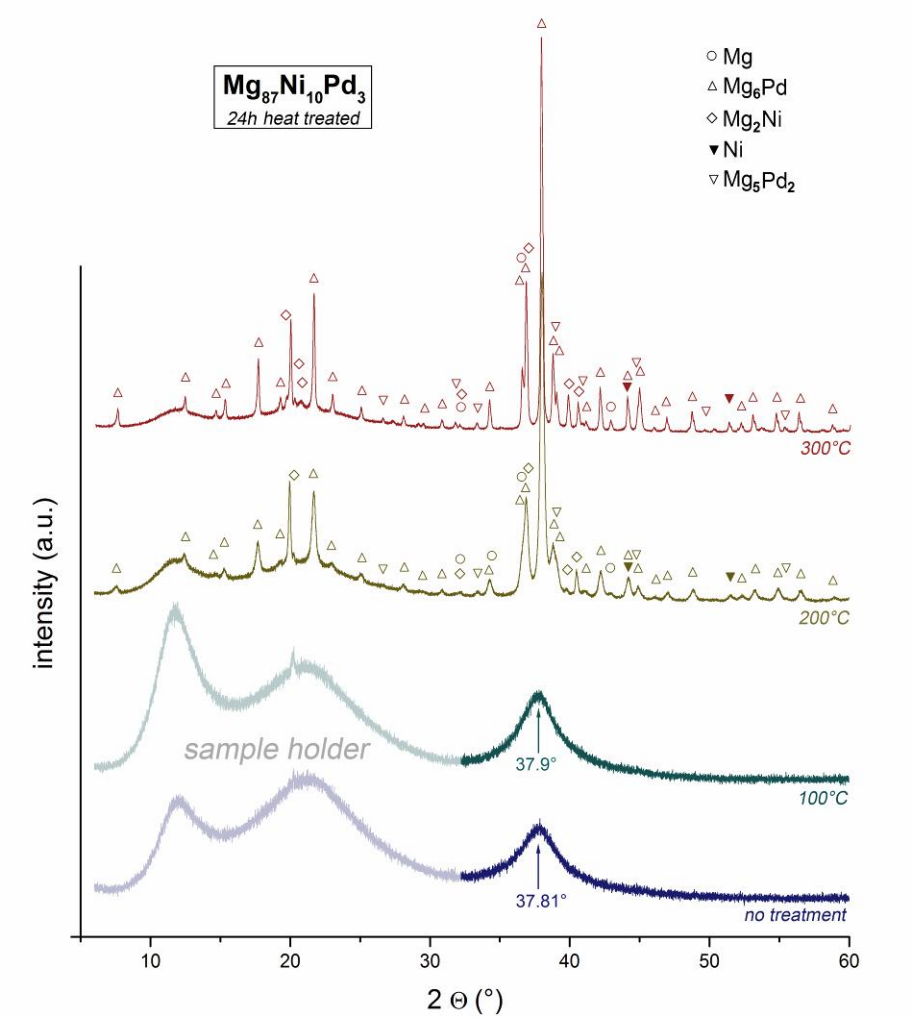

Fig. 6. XRD patterns of Mg-Ni-Pd sample heat treated at different temperatures in Ar atmosphere for 24 hours

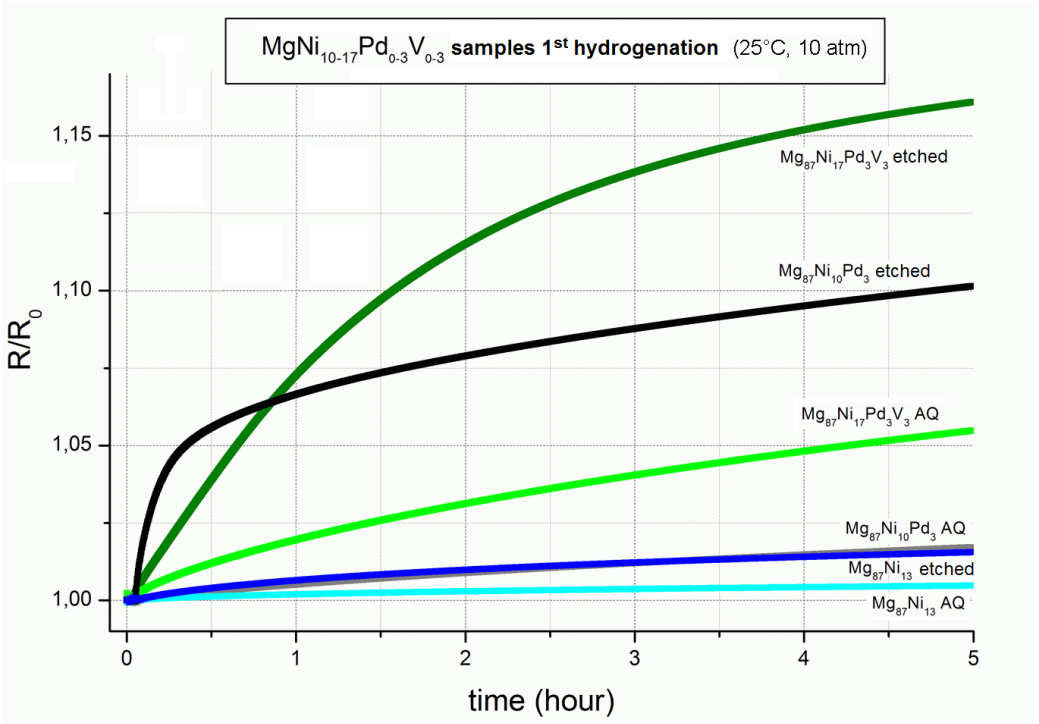

Fig. 7. First hydrogenation of activated (etched) and as-quenched (AQ) samples. Higher R/R_0 value indicates higher hydrogen content at a given composition (see [11]).

In the case of Mg-based alloys, the effect of these mechanisms is estimated to be lower, as Mg do not form a fluoride complex as Zr do, and Ni content of present alloys is lower. However, H-uptake was found to be significantly faster after surface activation, which points out, that there should be other effects of etching. The colorization of ribbon surfaces after treatment proves this assumption.

The found new effect of etching was introduced in our earlier article [11]. Now, that assumption was proved by further measurements. The basic principle is that a rapidly solidified amorphous ribbon contains structural inhomogeneties and stresses. A metastable state is hold up by the "frozen" diffusion. When etching, it turns into an unstable state by removing the surface layer of the ribbon, resulting a fast structural relaxation. This relaxation induces dilatations and contractions in the sample (which was determined quantitatively by precision length measurement – see Ref. [11]); and eventually, it causes the cracking of the surface. The better hydrogen permeability of cracked surface is well known from literature [12]. One further experiment was the heat treatment of etched samples: at higher temperature (100 °C) enhanced relaxation is expected which forces the above described effect.

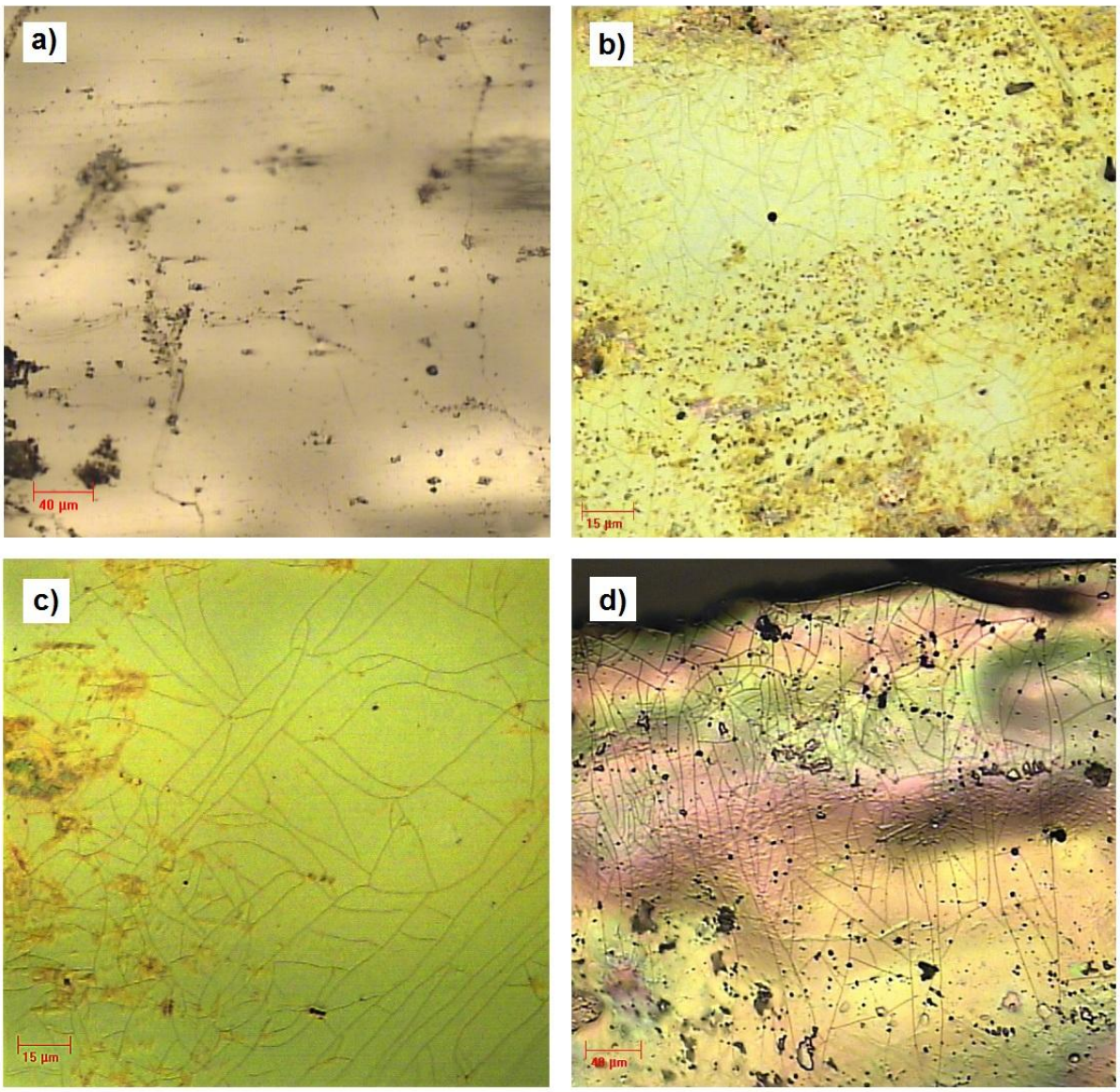

Fig. 8. Sample surfaces: $Mg_{87}Ni_{10}Pd_3$ as-quenched (a), etched (b), etched and heat treated at 100 °C (c) and $Mg_{77}Ni_{17}Pd_3V_3$ etched and heat treated at 100 °C (d) (full colour version available online)

The results proved this assumption: while only a slight surface cracking could be detected only at sample $Mg_{87}Ni_{10}Pd_3$ after etching, heat treatment resulted in a definitely stronger cracking at samples $Mg_{87}Ni_{10}Pd_3$ and $Mg_{85}(LaNi_5)_{15}$ too. As crystallization does not start at these samples at 100 °C, only structural relaxation can play role in this phenomenon. Reference measurements were also carried out with non-etched samples, which do not show such cracking effect; neither occurs it at crystalline ones (neither in etched nor in as-quenched state). Thus, it can be stated that *etching and structural relaxation together lead to surface cracking and – as a consequence – faster absorption*.

It should be added that – as one can see on Fig. 7 – etching has the stronger effect at $Mg_{87}Ni_{10}Pd_3$ sample (around 40 times higher absorption rate in the first 10 minutes in contrast with the 2.5 times higher rate of the other two samples). This ribbon is where the cracking could be observed without heat treatment. These results show that the effect of etching depends strongly on the relaxation tendency of the sample.

3.4. Surface processes during hydrogen absorption

Hydrogenation makes cracking effect more definite, and cracking occurs even at those amorphous samples where it could not be observed before hydrogenation. It is known from literature that the dilation of hydride phase opens up diffusion paths ensuring new, active surface for absorption [12]. Although hydride phase is formed only at crystalline samples, dilation and crack-opening phenomena occur at amorphous samples too during low temperature hydrogenation (without crystallization). The following surface processes can be identified in optical microscopic images:

During 100 °C hydrogenation a finely, homogenously crackled surface is formed (Fig. 9a). From this result, a homogenous relaxation and absorption process can be supposed without hydride phase formation. After hydrogenation at 300 °C wider cracks and hydride phase formation can be observed (Fig. 9b).

On some samples catalytically active "spots" (V and Pd-rich areas) were found, where fast hydrogen uptake and dilation causes strong cracking (Fig. 10a). After long hydrogenation at higher temperature, surface pitting can be seen on the surface (see Fig. 10b) – presumably due to the hydride phase formation at the previously mentioned active spots.

Strong hydride formation causes keen crinkling of the ribbon, and wide, opened strips are formed on the surface of $Mg_{87}Ni_{10}Pd_3$ sample after hydrogenation at 200 °C (Fig. 11).

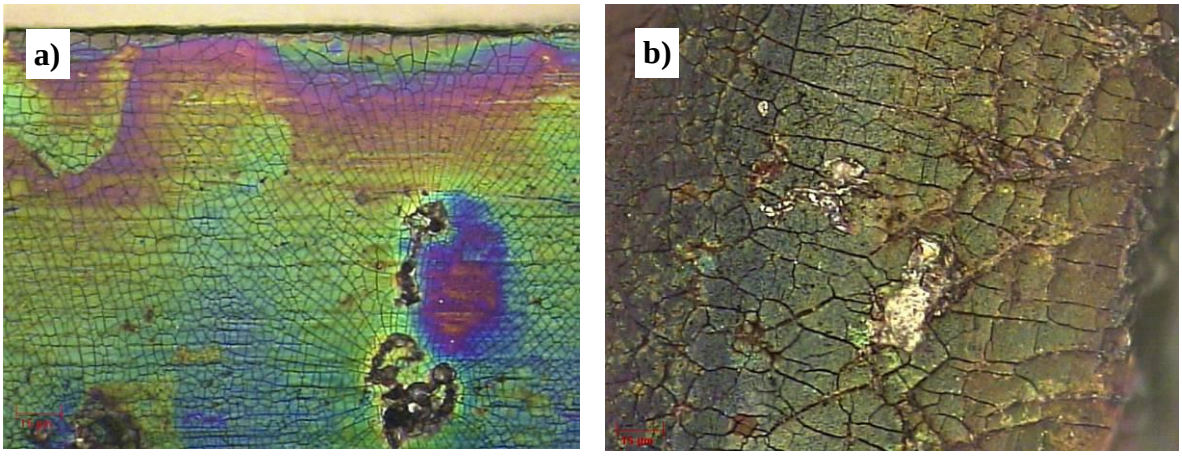

Fig. 9. Homogenously cracked $Mg_{87}Ni_{10}Pd_3$ ribbon – hydrogenated at 100 °C (a) and open cracks on $Mg_{77}Ni_{17}Pd_3V_3$ ribbon – hydrogenated at 300 °C (b) (full colour version available online)

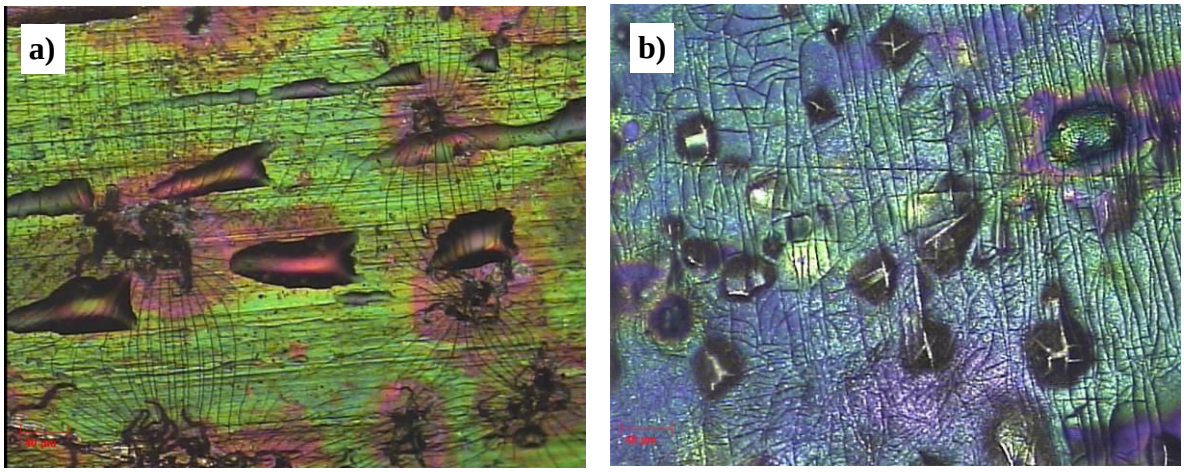

Fig. 10. "Active spots" on ribbon surface – $Mg_{77}Ni_{17}Pd_3V_3$ hydrogenated at 200 °C (a), hydride formation in active spots opens up surface layer – $Mg_{87}Ni_{10}Pd_3$ hydrogenated at 200 °C (b) (full colour version available online)

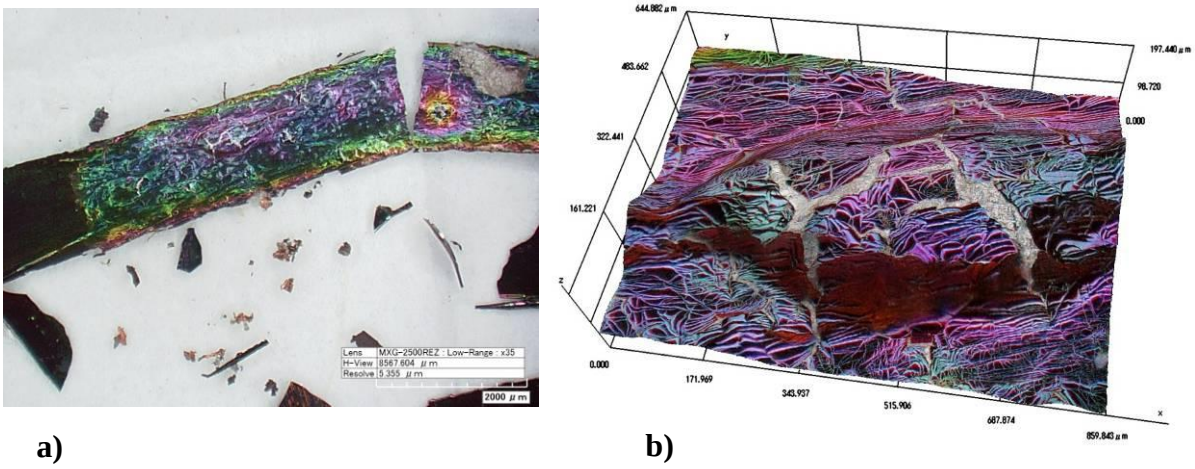

Fig. 11. Dilated hydride phase on the surface of the crinkled ribbon – $Mg_{87}Ni_{10}Pd_3$ hydrogenated at 200 °C

3.5. Bulk processes during hydrogen absorption

The examination of the effect of absorbed hydrogen on the crystallization and microstructure of samples was carried out via resistance and XRD measurements. In-situ resistance measurement results of hydrogenations and heat treatments (HT) at different temperatures are shown in Fig. 12, XRD patterns of the same samples – measured after hydrogenations – can be seen on Fig. 13.

In accordance with XRD results (Fig. 6.), resistance do not change significantly during heat treatment **at 100 °C**. It proves that no major structural change take place. However, a strong increase of resistance was registered at the hydrogenated sample due to hydrogen solution. XRD pattern of this sample shows around 10% nanocrystalline phases – mainly MgH_2. Further information can be reached from the position of the amorphous peak: it shifts towards the smaller angles (in contrast with the heat treated alloy) indicating the increase of average atomic distances due to solved hydrogen.

Treatment **at 200 °C** shows similar results in H as in Ar - beside the growing resistance increment of hydrogenated sample due to hydrogen solution. Qualitative difference in R/R_0 characteristic is only at the initial (heating) period. Despite the relatively small change of resistance during treatments, XRD measurements show a strong crystallization at

the heat treated sample (Fig. 6) as well as at the hydrogenated one (Fig. 13). The crystallized phases are the same – except ~ 5 % of hydride phases (Mg_2NiH_4 and MgH_2) in the hydrogenated sample. The rate of crystallization is higher due to hydrogen absorption: there remains only 9.5 % amorphous phase – around 5 % less, than in the heat treated sample. However, the still high resistance indicates that there is no continuous crystalline phase, but only nanocrystalline grains in an amorphous matrix are formed.

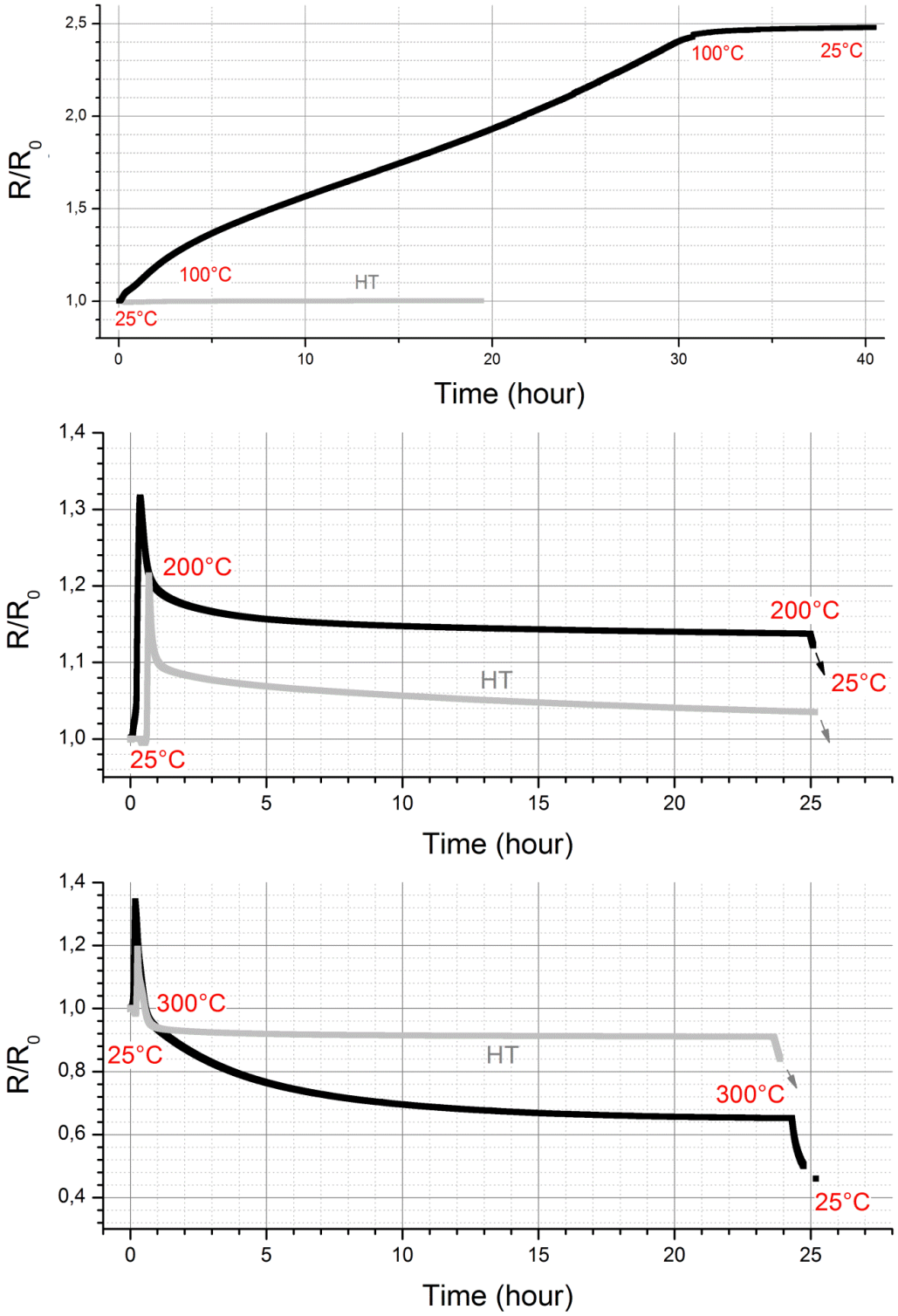

Fig. 12. Electric resistance normalized to initial value as a function of time during hydrogenation of $Mg_{87}Ni_{10}Pd_3$ sample at different temperatures and reference heat treatments (HT) carried out in Ar atmosphere at the same temperatures

Crystallization rate reaches the value of 95 % when treated **at 300 °C**. Though the XRD results of heat treated and hydrogenated samples are very similar (only ~ 0.5 % less amorphous phase and ~ 1.5 % hydride phases appears after hydrogenation), resistance measurement indicates a significant difference. The reason for this phenomenon could be the different process of crystallization: during heat treatment, a spontaneous, homogenous nucleus formation takes place, while absorbed hydrogen facilitates and enhances nucleus formation – as it is proved in [13] at Fe-Zr amorphous alloys and can be presumed from present results at 100 °C hydrogenation.

3.6. Absorption rate at different temperatures

The effect of temperature on absorption rate was quantitatively examined at $Mg_{77}Ni17Pd_3V_3$ sample. Main results are shown on Fig. 15. As one can see, fastest absorption can be achieved at 200 °C. The reason is composed of two effects: on the one hand, increasing temperature leads to faster processes in absorption kinetics (H-dissociation, diffusion, etc.). On the other hand, hydrogen diffusion in amorphous structure is much faster than in crystalline phase [14]. As a result, the increasing rate of crystallization with raising temperature leads to slower and slower diffusion. Real absorption rate will be evolved from the balance of these effects. Consequently, a temperature of 200 °C seems to be optimal by ensuring decent diffusion speed beside sufficiently low rate of crystallization.

4. Conclusions

We tailored and prepared Mg-based samples aiming the pure and efficient investigation of surface and bulk processes during hydrogenation at different temperatures. The most active absorbers were the Pd-containing samples (see [11]); further examinations were carried out mainly with those alloys.

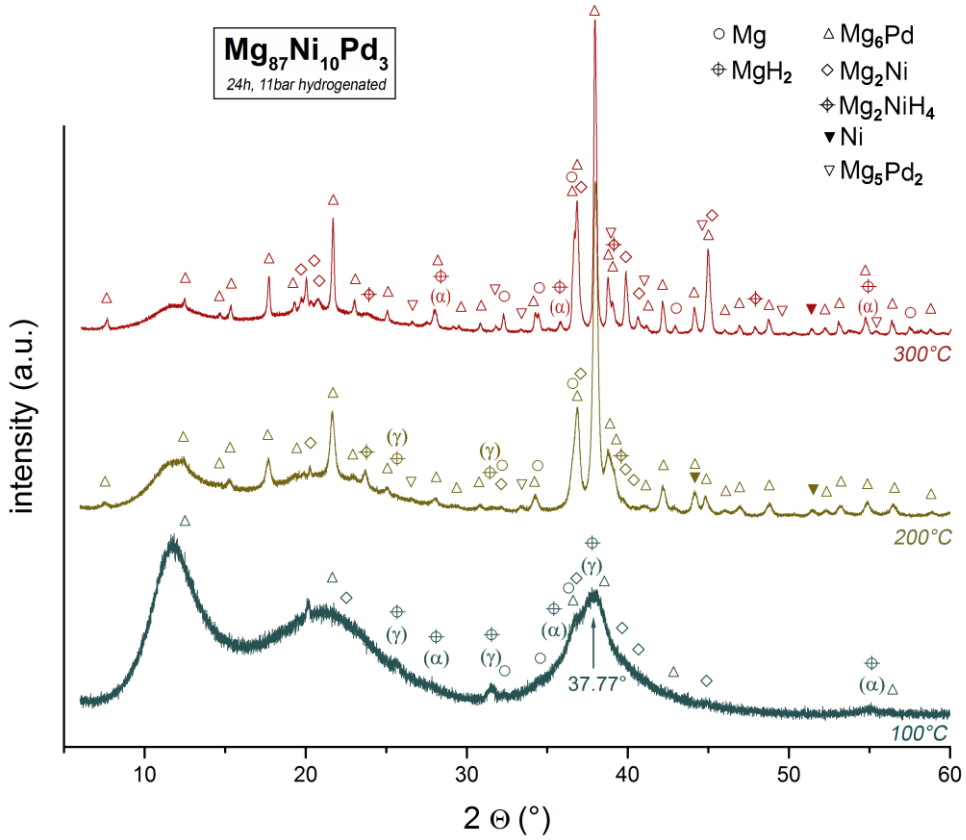

Fig. 13. XRD patterns of Mg-Ni-Pd samples hydrogenated at different temperatures for 24 hours

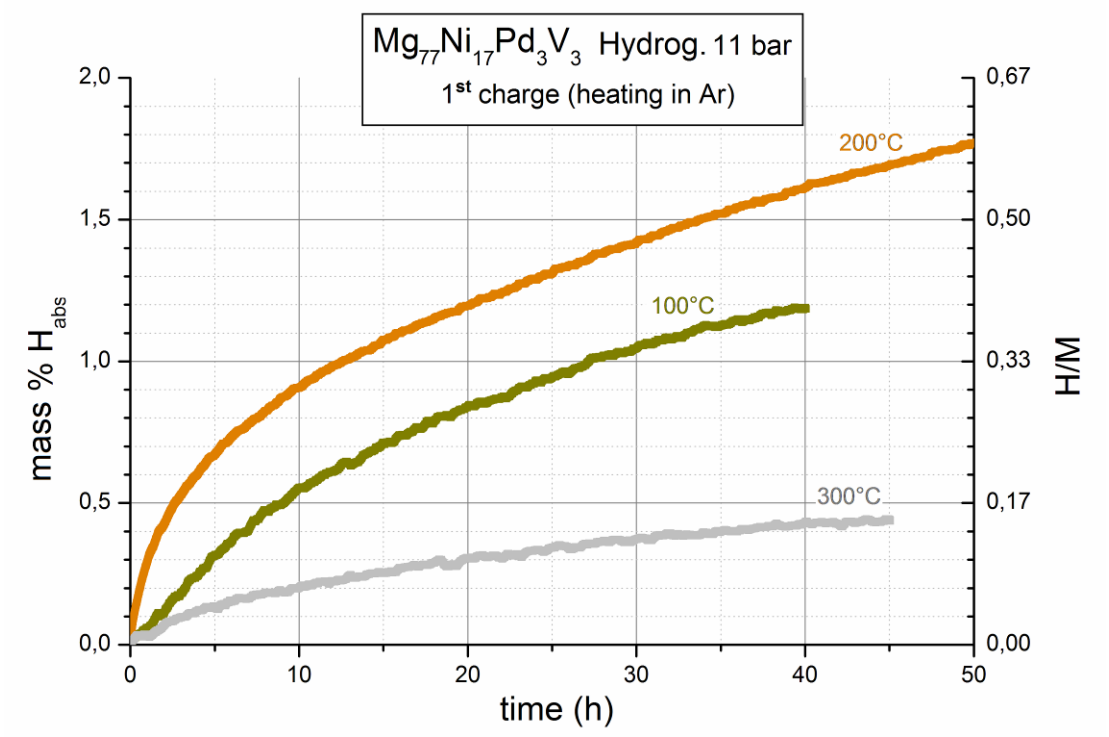

Fig. 14. Hydrogen absorption as a function of time at different temperatures

According to performed measurements and examinations, the following results were reached:

1. A new effect of etching amorphous alloys in HF solution was identified: enhanced relaxation leads to the cracking of the surface, resulting faster absorption.
2. We measured the density of different, Mg-based melt-spun alloys. Results pointed out that the density (free volume) of amorphous structures correlates with the equilibrium phases.
3. The thermal stability limits of different melt-spun alloys were determined during fast heating and long term heat treatment too. Results were verified via XRD measurements.
4. Surface processes during H-absorption at different temperatures were identified by optical microscopic examinations.
5. The effect of hydrogen on the crystallization process of amorphous Mg-based alloys was investigated via in-situ resistance measurement. We found, that hydrogen does not change significantly the microstructure of the samples at 100 and 200 °C as compared to heat-treated ones. However, hydrogen notably increases the rate of crystallization when treated at 300 °C.
6. The hydrogen absorption rates were determined at 100 – 200 – 300 °C. Fastest absorption was reached at 200 °C as an optimum between fast diffusion and low rate of crystallization.

Acknowledgements

This work is connected to the scientific program of "Development of quality-oriented and harmonized R + D + I strategy and functional model at BME" project. This project is supported by the New Hungary Development Plan (ID:TÁMOP-4.2.1/B-09/1/KMR-2010-0002).

The authors would like to acknowledge for the financial support to Hungarian Scientific Research Fund (OTKA) through grant No. K 73690.

References

[1] I.P.Jain, Chhagan Lal, Ankur Jain: Int. J. Hydrogen Energy 35 (2010) 5133-5144.

[2] L. Zaluski, A. Zaluska, P. Tessier, J. O. Ström-Olsen, R. Schulz: J. Alloys and Compounds 217 (1995) 295-300.

[3] B. Vehovszky, S. Balla: J. Machine Manufacturing XLIX. E3-E5 (2009) 35-38.

[4] M. Pasturel, R. J. Wijngaarden, W. Lohstroh, H. Schreuders, M. Slaman, B. Dam, R. Griessen: Chemistry of Mater. 19 (2007) 624-633.

[5] S. Kalinichenka, L. Röntzsch, B. Kieback: Int. J. Hydrogen Energy 34 (2009) 7749-7755.

[6] T. P. Blach, E. MacA. Gray: J. Alloys and Compounds 446–447 (2007) 692-697.

[7] M. Evening, J. Schewe: *Adobe Photoshop CS4 for Photographers*: The Ultimate Workshop (2009) 139-238.

[8] S. Nakano, S. Yamaura, S. Uchinashi, H. Kimura, A. Inoue: Sensors and Actuators – Chemical B 104 (2005) 75-79.

[9] D. Turnbull, M. H. Cohen: J. Chemical Phys. 34 (1961) 120-125.

[10] J. Garaguly: *Investigation of Hydrogen Absorption-desorption in Amorphous Alloys via In-situ Resistance Measurements* [PhD Thesis], BME Faculty of Transportation Engineering, MTA Institute for Solid State Physics and Optics, Budapest 1998.

[11] B. Vehovszky: Perner's Contacts VI Special Issue 2 (2011) 203-220.

[12] F. D. Manchester, D. Khatamian: Mater. Sci. Forum 31(1988) 261-296.

[13] B. Vehovszky, J. Kovác, P. Kamasa, Á. Cziráki: Mater. Sci. Forum 729 (2013) 509-514.

[14] T. Spassov, U. Koster: J. Alloys Comp. 287 (1999) 243-250.